C Journal of Carbon Research

MDPI

*Article*

# Power Generation Characteristics of Polymer Electrolyte Fuel Cells Using Carbon Nanowalls as Catalyst Support Material

**Takayuki Ohta [1,*], Hiroaki Iwata [1], Mineo Hiramatsu [1], Hiroki Kondo [2] and Masaru Hori [2]**

[1] Department of Electrical and Electronic Engineering, Meijo University, 1-501 Shiogamaguchi, Tempaku, Nagoya 468-8502, Japan
[2] Center for Low-Temperature Plasma Sciences, Nagoya University, Furo, Chikusa, Nagoya 464-8603, Japan
* Correspondence: tohta@meijo-u.ac.jp

**Abstract:** We evaluated the power generation characteristics of a polymer electrolyte fuel cell (PEFC) composed of Pt-supported carbon nanowalls (CNWs) and a microporous layer (MPL) of carbon black on carbon paper (CP) as catalyst support materials. CNWs, standing vertically on highly crystallizing graphene sheets, were synthesized on an MPL/CP by plasma-enhanced chemical vapor deposition (PECVD) using inductively coupled plasma (ICP). Pt nanoparticles were supported on the CNW surface using the liquid-phase reduction method. The three types of voltage loss, namely those due to activated polarization, resistance polarization, and diffusion polarization, are discussed for the power generation characteristics of the PEFC using the Pt/CNWs/MPL/CP. The relationship between the height or gap area of the CNWs and the voltage loss of the PEFC is demonstrated, whereby the CNW height increased with the extension of growth time. The three-phase interface area increased with the increase in the CNW height, resulting in mitigation of the loss due to activated polarization. The gap area of the CNWs varied when changing the $CH_4/H_2$ gas ratio. The loss due to diffusion polarization was reduced by enlarging the gap area, due to the increased diffusion of fuel gas and discharge of water. The secondary growth of the CNWs caused the three-phase interface area to decrease as a result of platinum aggregation, impedance of the supply of ionomer dispersion solution to the bottom of the CNWs, and inhibition of fuel gas and water diffusion, which led to the loss of activated and diffuse polarizations. The voltage losses can be mitigated by increasing the height of CNWs while avoiding secondary growth.

**Keywords:** polymer electrolyte fuel cell; carbon nanowalls; plasma-enhanced chemical vapor deposition

check for updates

**Citation:** Ohta, T.; Iwata, H.; Hiramatsu, M.; Kondo, H.; Hori, M. Power Generation Characteristics of Polymer Electrolyte Fuel Cells Using Carbon Nanowalls as Catalyst Support Material. *C* **2022**, *8*, 44. https://doi.org/10.3390/c8030044

Academic Editors: Olena Okhay and Gil Goncalves

Received: 7 July 2022
Accepted: 22 August 2022
Published: 27 August 2022

**Publisher's Note:** MDPI stays neutral with regard to jurisdictional claims in published maps and institutional affiliations.

**Copyright:** © 2022 by the authors. Licensee MDPI, Basel, Switzerland. This article is an open access article distributed under the terms and conditions of the Creative Commons Attribution (CC BY) license (https://creativecommons.org/licenses/by/4.0/).

## 1. Introduction

Polymer electrolyte fuel cells (PEFCs) have been applied as power sources in cogeneration systems and vehicles due to their compact size and low operating temperature. However, the improvement of their power generation efficiency and ensuring the high durability of electrode material are needed. The structure of the fuel cell is sandwich-like, where there is a catalyst layer (CL) and gas diffusion layer (GDL) on either side of the proton exchange membrane in addition to another catalyst layer. The CL is essential for accelerating the oxygen reduction reaction (ORR), which is slow. The morphological features (shape/size and porosity) of the catalyst determines its degree of dispersion and accessibility to protons and oxygen/hydrogen. The GDL is also an important component in the PEFC, and the main function of the GDL is to transfer water and gas. Accordingly, the interaction with the catalyst can affect the catalyst electronic energy, thereby affecting the kinetics. Carbon nanoparticle-based platinum catalysts have been widely used, which comprise platinum nanoparticles (2–5 nm) supported on carbon black nanoparticles (20–30 nm) covered with a nanothin film of ionomer. The modification of carbon support materials for Pt and Pt-alloy cathode catalysts has been reported to successfully improve the performance and durability of PEFCs. The criteria for use as a support material are as follows: (1) sufficient electrical conductivity; (2) large surface area; (3) high resistance to electrochemical

corrosion; (4) suitable porosity and a porous structure; (5) strong stability in acidic or alkaline media; (6) adequate proton conductivity; (7) sufficient compatibility with electrodes; (8) adequate water handling to avoid flooding; and (9) strong interaction between the support and the catalyst. The following have been reported as new carbon-based materials: carbon black [1–12], mesoporous carbon [13–19], carbon nanotubes (CNTs) [10,12,13,20–28], hollow graphite spheres [29,30], carbon cloth [31], graphene [32–38], carbon nanofibers (CNFs) [9,13,21,39–43], carbon aerogels [13,44], carbon xerogel [45–49], carbon nanocoils (CNCs) [5,50–55], fullerene [56–58], carbon nano-onions [59,60], carbon nanohorn [61,62], and polymer-based nanohybrids [63]. In addition, the following noncarbon-supported materials have been developed: Pt/Ta-$SnO_2$ [64], Pt–Co/C [65], Fe–N–C catalyst [66], and silica-coated Pt [67].

In recent years, carbon nanowalls (CNWs) were discovered, and fundamental research on them has been progressing [68–71]. CNWs have been grown using various chemical vapor deposition (CVD) methods, and several applications using CNWs have been reported, such as fuel cells [72–77], biofuel cells [78], strain sensors [79], electrochemical sensors [80–82], scaffolds [83], and substrates for surface-assisted laser desorption/ionization mass spectrometry [84,85]. CNWs are composed of stacked graphene sheets and are stranded perpendicular to the substrate. CNWs are expected to be alternative catalyst support materials due to their high electric conductivity, very large specific surface area, and physically robust shape due to having a high aspect ratio. The electrochemical characterization or high durability of CNWs for a fuel cell has been reported [77–81]. A test cell unit using a Pt-supported CNW/carbon fiber paper was fabricated and the V–I curve characterized for assessment of proton exchange membrane (PEM) fuel cell application. However, the PEM fuel cell exhibits a voltage drop to 0.2 V due to activated polarization, because no ionomer binder is incorporated in the catalyst layers. The three-phase boundary region near the surface of the catalyst layers and the proton conduction between the catalyst layer and membrane are both essential for improving the power generation efficiency. Since CNWs have a unique structure, the gap area and height of CNWs can be controlled by changing the deposition conditions.

In this study, CNWs were synthesized on a microporous layer (MPL) of carbon black on carbon paper (CP) by plasma-enhanced chemical vapor deposition (PECVD) using inductively coupled plasma (ICP) to improve the power generation of the PEFC. The relationship between the CNW height or gap area and the PEFC power generation characteristics was investigated.

## 2. Materials and Methods

### *2.1. Plasma-Enhanced Chemical Vapor Deposition for CNW Growth*

Figure 1 shows a schematic diagram of the ICP reactor used for CNW growth. RF (13.56 MHz) power was applied to the coil antenna. Two types of CNWs with different gap spaces between walls were synthesized on an MPL of carbon black on the CP (MPL/CP) (SGL carbon GmbH; GDL 29BC, thickness: 235 μm, void fraction: 40–41%). Condition (1) for the small gap was 550 W RF power, 20/44 sccm $Ar/CH_4$ gas flow rates, 22 mTorr total pressure, and 720 °C growth temperature. Condition (2) for the large gap was 600 W RF power, 20/9/8 sccm $Ar/CH_4/H_2$ gas flow rates, 16 mTorr total pressure, and 720 °C growth temperature.

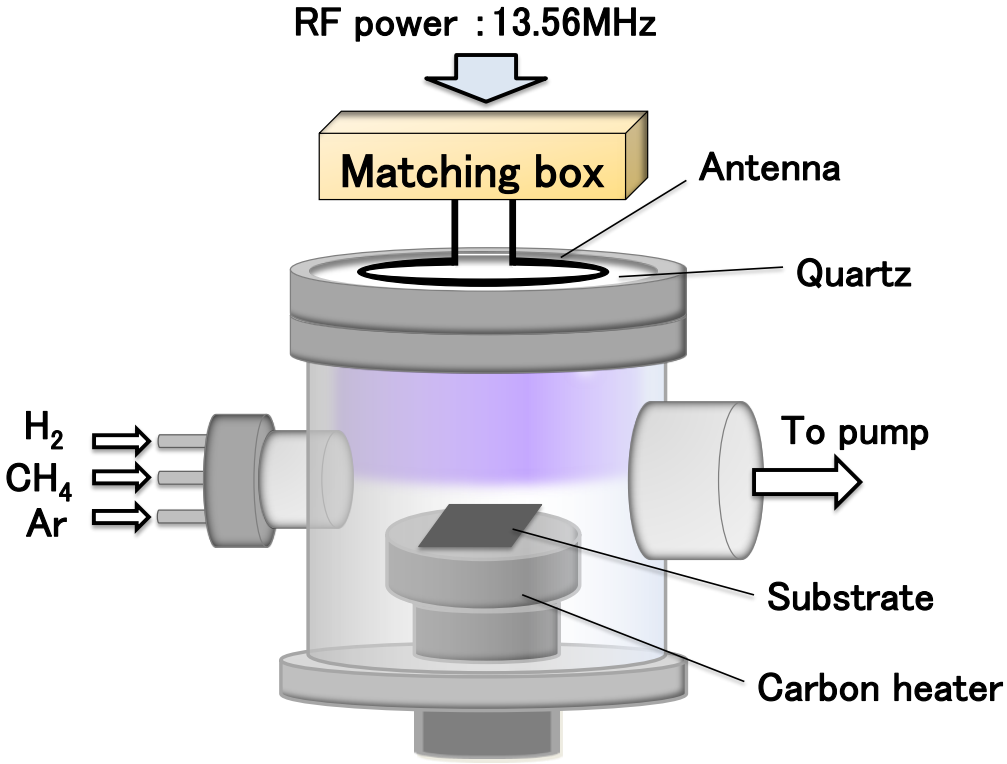



**Figure 1.** Schematic diagram of the ICP reactor.

*2.2. Structure of a Single PEFC Using CNWs*

Figure 2 shows a schematic diagram of the single PEFC, which was assembled with a membrane electrode assembly (MEA) and separators. The MEA consisted of the Pt-supported CNWs on MPL/CP, ionomer dispersion solution, and non-treated ionomer membrane (Nafion 117) for proton exchange. The surface of the CNWs on the MPL/CP was treated with atmospheric pressure plasma to endow hydrophilicity. The Ar gas flow rate was 2.0 sccm, the applied voltage to the electrodes was 6 kV, and the treatment distance was 5 mm. Pt nanoparticles were supported on the surface of the CNWs/MPL/CP by the liquid-phase reduction method using chloroplatinic acid solution ($H_2PtCl_6$, 8 wt.% in $H_2O$) and $NaBH_4$ as the reducing agents. A total volume of 0.1 mL ionomer dispersion solution (Nafion DE202) diluted with 2-propanol was applied dropwise on the Pt/CNWs/MPL/CP. The MEA was fabricated by hot-pressing at 135 °C with a pressing pressure of 5.0 MPa and pressing time of 90 s. The MEA with an electrode area of 5 $cm^2$ was assembled to the standard single PEFC (Electro Chem, Inc., EFC-05-02, Woburn, MA, USA). The power generation characteristics were investigated using a fuel cell test system (Scribner Associates Inc., AutoPEM, Southern Pines, NC, USA) at an anode $H_2$ gas flow rate of 0.1 L/m, cathode air flow rate of 0.2 L/m, and a temperature of 80 °C.

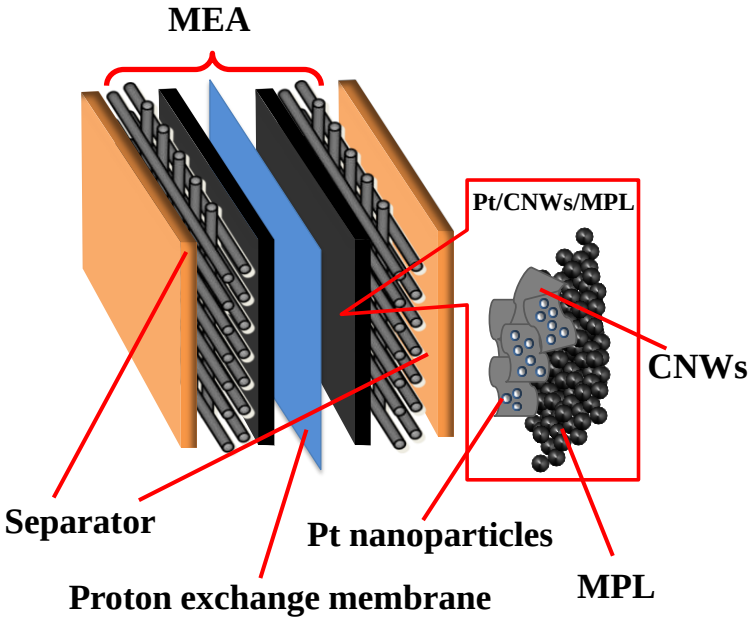



**Figure 2.** Schematic diagram of the single PEFC using CNWs.

## 3. Results and Discussion

### *3.1. CNWs on MPL/CP*

Figure 3 shows the height of the CNWs as a function of the growth time for condition (1). The height of the CNWs increased from 1.7 μm to 7.2 μm as the growth time increased. The growth rate was estimated as 28 nm/min. Figure 4 shows the SEM images of the CNWs for various growth times. The CNWs were directly formed on the MPL of carbon black as shown in Figure 4a. The growth mechanism of CNWs on the substrates was detailed in a previous report [80]. The growth was as follows: (1) A very thin amorphous carbon layer formed on the substrate. (2) A nucleation site was formed there by ion irradiation. (3) Nanoislands were formed by aggregating carbon radicals at the nucleation site. (4) The nanoislands were irradiated with ions, and the absorption of carbon radicals was enhanced. (5) Nanographene grew preferentially in the height direction to form carbon nanowalls. In this study, the flake-like CNWs grew on the MPL, and some branches grew from the flake-like CNWs after 3 h.

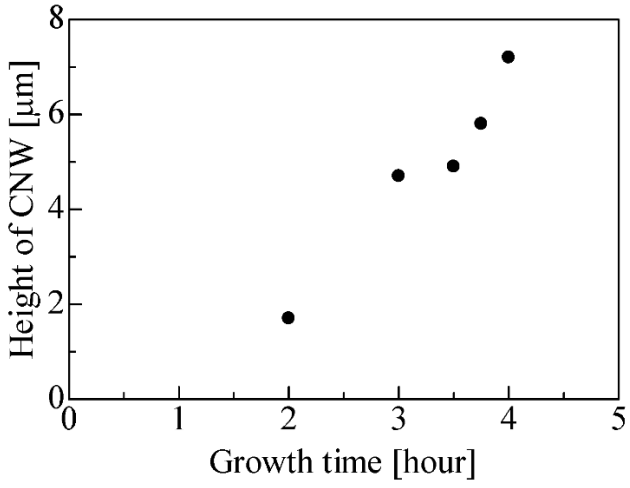
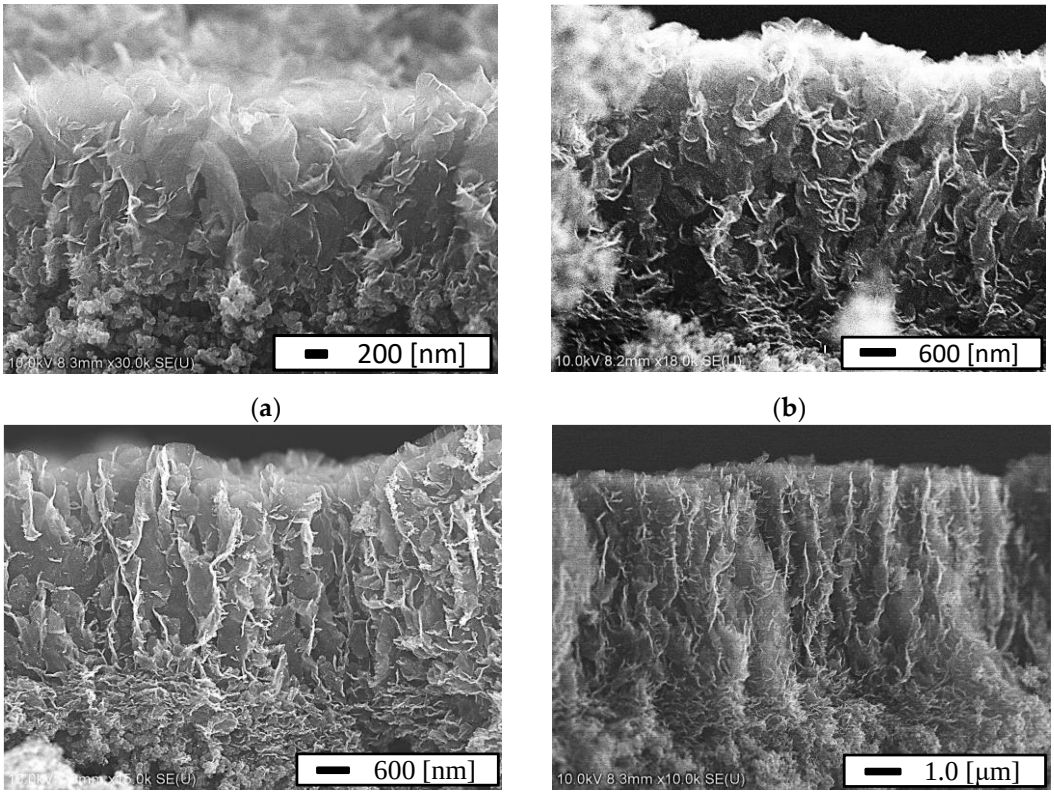



**Figure 3.** Height of CNW as a function of growth time.




(**a**) (**b**) (**c**) (**d**)

**Figure 4.** Cross-sectional view of the SEM images of the CNWs at a growth time of (**a**) 2 h, (**b**) 3 h, (**c**) 3.5 h, and (**d**) 4 h.

### *3.2. Relationship between CNW Height and Power Generation Characteristics*

Figure 5 shows the voltage–current density (V–J) curve of the single PEFC for the various growth times for deposition under condition (1). Three gradients, due to activated polarization, resistance polarization, and diffusion polarization, were observed on the PEFC using Pt/CNW/MPL/CP. The maximum current density increased with the increase in the growth time up to 3.5 h, since the reaction area at the three-phase boundary region among Pt on CNW, ionomer dispersion solution, and supplied fuel gas increased with the increase in the CNW height. The maximum current density, however, decreased after more than 3.5 h, because the dispersion of the Pt and ionomer dispersion solution to the bottom of CNWs was suppressed due to the secondary growth (branches) from the sidewalls of the flake-like CNWs.

The magnitude of the three types of voltage loss, activated polarization, resistance polarization, and diffusion polarization, was evaluated with consideration to the power generation characteristics and how improvements could be achieved by reducing this loss [86]. Figure 6 shows the voltage loss due to activated polarization for the various growth times. Activated polarization is the potential difference beyond the value of equilibrium needed to generate currents and is dependent on the energy activation of a redox reaction and its reaction area, and it can be calculated using the following equations:

$$\eta_a = a + b \log i \tag{1}$$

$$a = -\frac{2.303RT}{\alpha nF} \log i_0 \tag{2}$$

$$b = \frac{2.303RT}{\alpha nF} \log i \tag{3}$$

$$i_0 = nFAck_0 \exp\left(\frac{-E_a}{RT}\right) \quad (4)$$

where $i$ is the total current (A), $a$ is the coefficient of migration, $R$ is the gas constant (8.314 J/K mol), $T$ is the temperature (K), $i_0$ is the exchange current (A), $n$ is the number of electrons involved in the reaction (mol), $F$ is the Faraday constant (96,485 C/mol), $E_a$ is the activation energy (J/mol), $k_0$ is the reaction rate constant ($s^{-1}$), and $A$ is the reaction area ($m^2$).

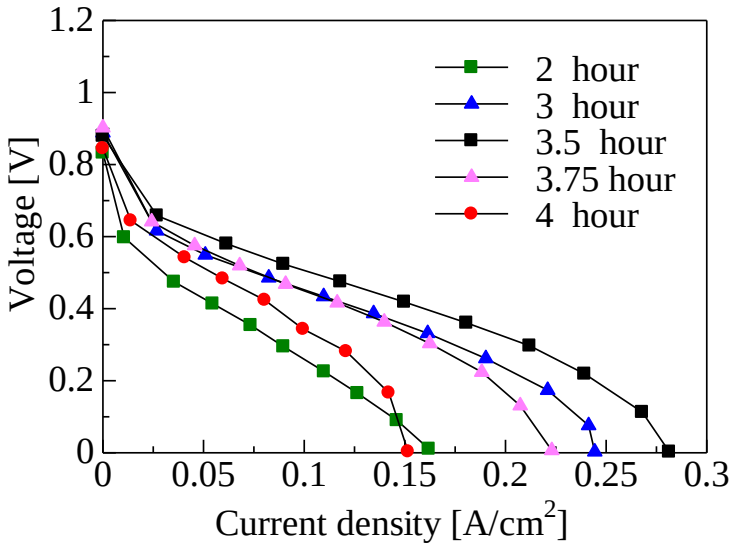



**Figure 5.** Voltage–current density (V–J) curve of single PEFC cells of Pt/CNW/MPL/CP for various growth times of the CNWs.

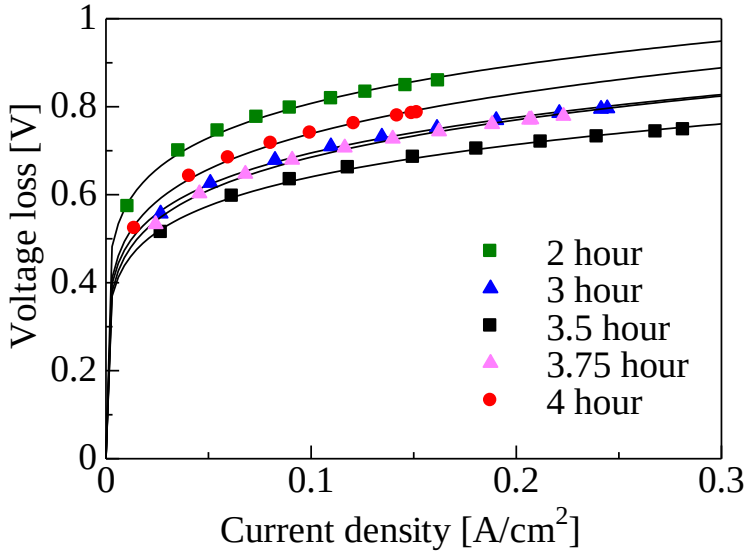



**Figure 6.** Activated polarization for various growth times.

The loss due to activated polarization decreased as the growth time was increased from 2 to 3.5 h, followed by an increase from 3.5 to 4 h. The activation energy remained constant in this study because the catalytic activity did not change for any of the experimental conditions. As shown in Figure 3, the three-phase interface region increased with the increase in CNW height observed from 2 to 3.5 h, resulting in an increase in reaction area $A$. However, the Pt particles aggregated due to CNW secondary growth from 3.5 to 4 h. Accordingly, the decrease in the three-phase interface led to the loss of activated polarization.

Figure 7 shows the voltage loss due to resistance polarization for the various growth times. Resistance polarization is a part of electrode polarization arising from an electric current through an ohmic resistance within the electrode or the electrolyte. The resistance polarization can be calculated using the following equation:

$$\eta_r = jRa \tag{5}$$

where $j$ is the current density (A/cm$^2$) and $R$ is the internal resistance of the fuel cell ($\Omega$cm$^2$). The ionic conductivity of the electrolyte, the electrical conductivity of the CNWs, and the contact resistance did not change regardless of the CNW growth time.

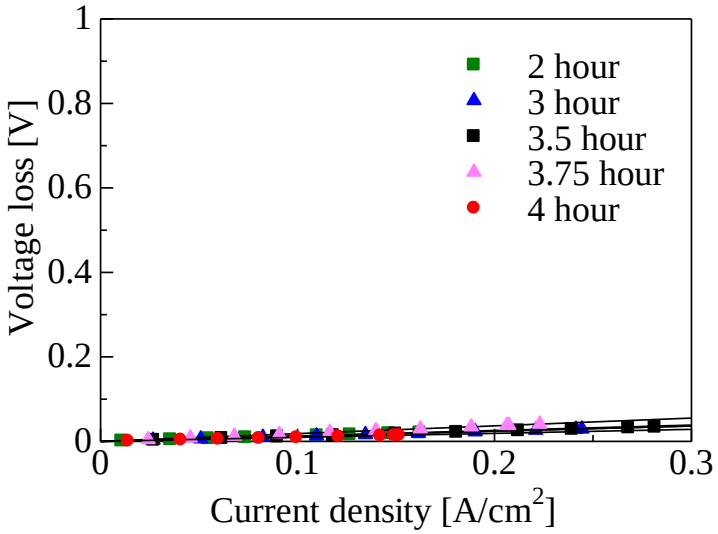



**Figure 7.** Resistance polarization for various growth times.

Figure 8 shows the voltage loss due to diffusion polarization for the various growth times. The diffusion polarization of an electrode is a result of the formation of a diffusion layer for fuel gas at the three-phase boundary or the water as a byproduct of an oxygen reduction reaction. Diffusion polarization can be calculated using the following equation:

$$\eta_d = -b \log \frac{C_{OX}}{C^{\circ}{}_{OX}} \tag{6}$$

where $C_{OX}$ is the concentration of oxygen at the three-phase boundary and $C^{\circ}{}_{OX}$ is the concentration of bulk oxygen. The loss due to diffusion polarization decreased with the increase in growth time from 2 to 3.5 h, since the oxygen concentration ($C_{OX}$) at the three-phase boundary increased along with the CNW height. However, from 3.5 to 4 h, the loss due to diffusion polarization decreased. The supply of fuel gas to the three-phase interface or the discharge of water molecules as the byproduct of the oxygen reduction reaction would be suppressed by CNW secondary growth. It was found that the best power generation characteristics were obtained at the growth time of 3.5 h, as shown in Figure 5, due to an increase in the three-phase interface area and the improvements such as the increased diffusion of fuel gas and water molecules.

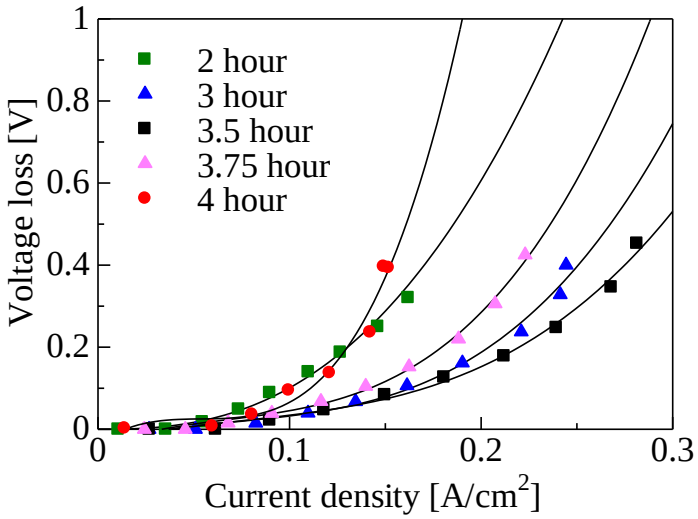



**Figure 8.** Diffusion polarization for various growth times.

### *3.3. Relationship between CNW Gap Area and Power Generation Characteristics*

Figure 9 shows plane or cross-sectional SEM images of the CNWs for different gap areas. The CNWs with a small gap area (0.37 μm$^2$) were deposited under condition (1), and those with a large gap area (0.79 μm$^2$) were obtained under condition (2). The growth time to achieve a height of 1.6 μm was 2 h for condition (1) and 70 min for condition (2) since the influence of the secondary growth can be suppressed under relatively low height. Here, the gap area of CNWs was evaluated from the area enclosed by the walls as their reciprocal [87].

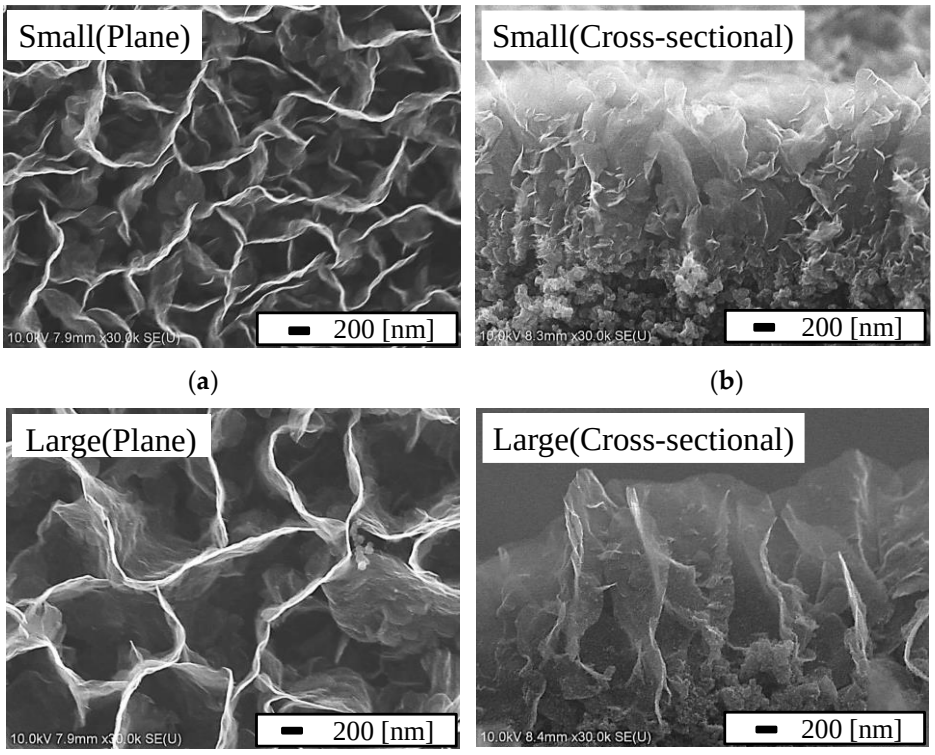



**Figure 9.** (**a**,**c**) Plane view and (**b**,**d**) cross-sectional view of the SEM images of CNWs grown on MPL with (**a**,**b**) a small gap area (0.37 μm$^2$) and (**c**,**d**) a large gap area (0.79 μm$^2$).

Figure 10 shows the V–J curve of a single PEFC for the different gap areas. Three gradients, due to activated polarization, resistance polarization, and diffusion polarization, were observed on the large gap area. The voltage of approximately 0.91 V at a current density of 0 mA/cm$^2$ was obtained for a large gap area under relatively low height. Moreover, the maximum current density for a large gap area was larger than that with a small gap area and was increased from approximately 0.15 to 0.3 A/cm$^2$ at the same height. Figure 11 shows the voltage loss due to activated polarization for the different gap areas. The voltage loss due to the activated polarization for the large gap was smaller than that for the small gap. The difference was approximately 0.2 V regardless of the current density. These results indicate that the three-phase interface region increased with the increase in gap area since the supply of platinum or ionomer dispersion solution to the bottom of the CNWs may have been enhanced. Figure 12 shows the voltage loss due to diffusion polarization for the different gap areas. The voltage loss due to diffusion polarization for the large gap was improved to be approximately 4 times smaller than that for the small gap. This result indicates that the supply of fuel gas to the three-phase interface and the discharge of water molecules were drastically improved by enlarging the gap of CNWs.

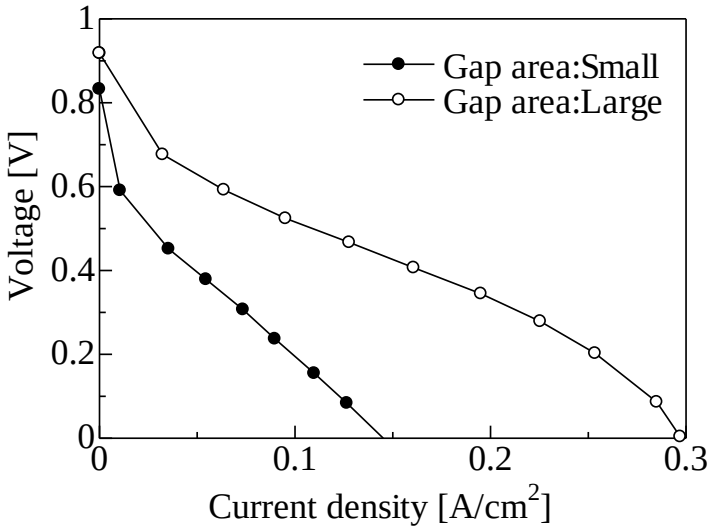



**Figure 10.** Voltage–current density (V–J) curve of single PEFC cells of Pt/CNWs/MPL/CP for different gap areas.

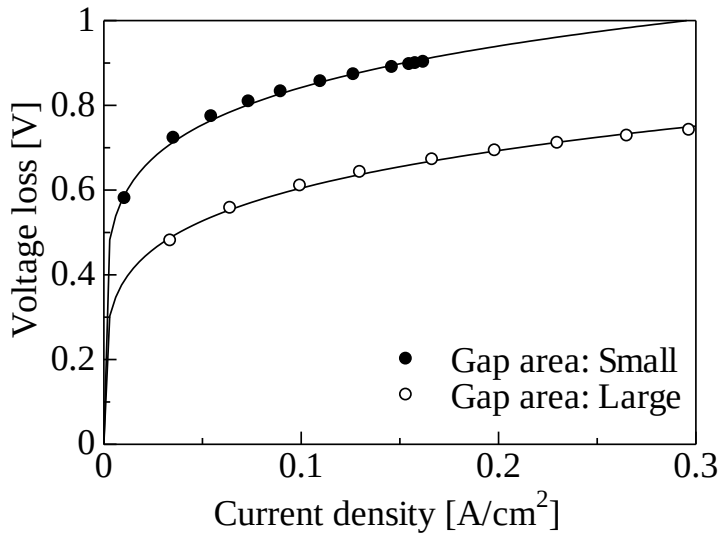



**Figure 11.** Activated polarization for different gap areas.

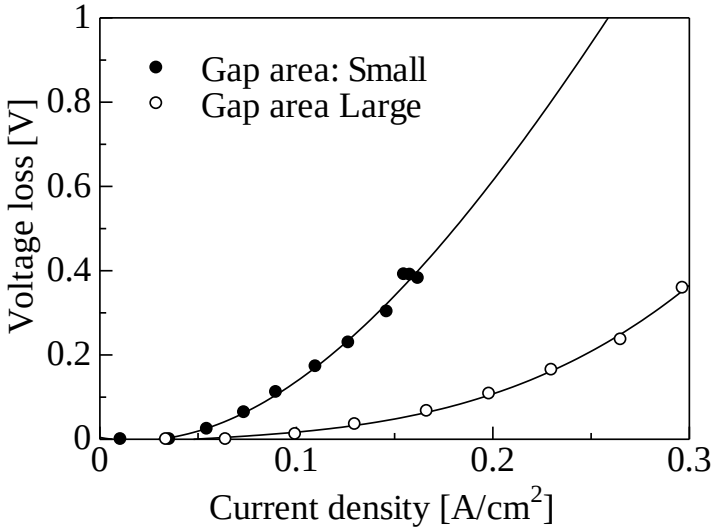



**Figure 12.** Diffusion polarization for different gap areas.

The voltage loss due to activated polarization and diffusion polarization was improved by an increase in gap area, although the surface area of the CNWs was decreased. The improvement in the diffusion polarization indicates that the supply of fuel gas to the three-phase interface and the discharge of water molecules were enhanced. Accordingly, the loss due to the activated polarization was improved, since the effective area of the three-phase interface was increased by the supply of fuel gas. Moreover, the Pt particle and the ionomer dispersion solution would be supplied to the bottom of CNWs in the case of the large gap. It was found that the power generation characteristics were improved by enlarging the gap of CNWs, since the loss due to activated polarization and diffusion polarization was mitigated.

## 4. Conclusions

CNWs as catalyst support materials were synthesized on an MPL/CP by ICP-PECVD. The power generation of the single PEFC using Pt/CNWs/MPL/CP as an MEA was demonstrated. The power generation characteristics of the PEFC were evaluated based on the three types of voltage loss due to activated polarization, resistance polarization, and diffusion polarization.

- An increase in the height of the CNWs increased the three-phase interface area with a reduction in the loss due to activated polarization.
- An increase in the gap area of the CNWs resulted in improvements due to increases in fuel gas diffusion and water discharge, and the loss due to diffusion polarization was reduced.
- The secondary growth of the CNWs caused a reduction in the three-phase interface area due to platinum aggregation, impedance of the supply of ionomer dispersion solution to the bottom of CNWs, and inhibited fuel gas and water diffusion, which led to the loss of activated and diffuse polarizations.

The voltage losses can be mitigated by increasing the height of the CNWs and expanding the gap area. The data obtained in this study are useful for the fabrication of PEFCs using CMWs.

**Author Contributions:** Conceptualization, investigation and writing—original draft preparation, T.O., data curation, H.I.; supervision, resources and project administration, H.K., M.H. (Masaru Hori) and M.H. (Mineo Hiramatsu). All authors have read and agreed to the published version of the manuscript.

**Funding:** This work was partly supported by the project for promoting research in Meijo University.

**Institutional Review Board Statement:** Not applicable.

**Informed Consent Statement:** Not applicable.

**Data Availability Statement:** Not applicable.

**Conflicts of Interest:** The authors declare no conflict of interest.

## References


1. Clingerman, M.L.; Weber, E.H.; King, J.A.; Schulz, K.H. Synergistic effect of carbon fillers in electrically conductive nylon 6,6 and polycarbonate based resins. *Polym. Compos.* **2002**, *23*, 911–924. [CrossRef]
2. Rimbu, G.A.; Jackson, C.L.; Scott, K. Platinum/carbon/polyaniline based nanocomposites as catalysts for fuel cell technology. *J. Optoelectron. Adv. Mater.* **2006**, *8*, 611–616.
3. Tang., S.; Sun, G.; Qi, J.; Sun, S.; Guo, J.; Xin, Q. Review of new carbon materials as catalyst supports in direct alcohol fuel cells. *Chin. J. Catal.* **2010**, *3*, 12–17. [CrossRef]
4. Lavacchi, A.; Miller, H.; Vizza., F. *Nanostructure Science and Technology*; Springer: New York, NY, USA, 2013.
5. Celorrio, V.; Flórez-Montaño, J.; Moliner, R.; Pastor, E.; Lázaro, M.J. Fuel cell performance of Pt electrocatalysts supported on carbon nanocoils. *Int. J. Hydrogen Energy.* **2014**, *39*, 5371–5377. [CrossRef]
6. Kaluža, L.; Larsen, M.J.; Zdražil, M.; Gulková, D.; Vít, Z.; Šolcová, O.; Soukup, K.; Koštejn, M.; Bonde, J.L.; Maixnerová, L.; et al. Highly loaded carbon black supported Pt catalysts for fuel cells. *Catal. Today* **2015**, *256*, 375–383. [CrossRef]
7. Fujii, K.; Ito, M.; Sato, Y.; Takenaka, S.; Kishida, M. Performance and durability of carbon black-supported Pd catalyst covered with silica layers in membrane electrode assemblies of proton exchange membrane fuel cells. *J. Power Sources* **2015**, *279*, 100–106. [CrossRef]
8. Lee, W.H.; Seo, J.; Lee, T.; Kim, H. Preparation of a self-assembled organosilane coating on carbon black as a catalyst support in polymer electrolyte membrane fuel cells. *J. Power Sources* **2015**, *274*, 1140–1146. [CrossRef]
9. Li, M.; Wu, X.; Zeng, J.; Hou, Z.; Liao, S. Heteroatom doped carbon nanofibers synthesized by chemical vapor deposition as platinum electrocatalyst supports for polymer electrolyte membrane fuel cells. *Electrochim. Acta* **2015**, *182*, 351–360. [CrossRef]
10. Geraldes, A.N.; Furtunato da Silva, D.; Martins da Silva, J.C.; Antonio de Sá, O.; Spinacé, E.V.; Neto, A.O.; Coelho dos Santos, M. Palladium and palladium—Tin supported on multi wall carbon nanotubes or carbon for alkaline direct ethanol fuel cell. *J. Power Sources.* **2015**, *275*, 189–199. [CrossRef]
11. Zhou, K.; Li, T.; Han, Y.; Wang, J.; Chen, J.; Wang, K. Optimizing the hydrophobicity of GDL to improve the fuel cell performance. *RSC Adv.* **2021**, *11*, 2010. [CrossRef]
12. Quan, D.L.; Le, P.H. Enhanced methanol oxidation activity of PtRu/$C_{100-x}$MWCNTs$_x$ (x = 0–100 wt.%) by controlling the composition of C-MWCNTs support. *Coatings* **2021**, *11*, 571. [CrossRef]
13. Antolini, E. Carbon supports for low-temperature fuel cell catalysts. *Appl. Catal. B Environ.* **2009**, *88*, 1–24. [CrossRef]
14. Liu, H.-J.; Cui, W.-J.; Jin, L.-H.; Wang, C.-X.; Xia, Y.-Y. Preparation of three-dimensional ordered mesoporous carbon sphere arrays by a two-step templating route and their application for supercapacitors. *J. Mater. Chem.* **2009**, *19*, 3661–3667. [CrossRef]
15. Tang, Z.-H.; He, X.; Song, Y.; Liu, L.; Guo, Q.-G.; Yang, J.-H. Properties of mesoporous carbons prepared from different carbon precursors using nanosize silica as a template. *N. Carbon Mater.* **2010**, *25*, 465–469. [CrossRef]
16. Li, Y.; Fu, Z.-Y.; Su, B.-L. Hierarchically structured porous materials for energy conversion and storage. *Adv. Funct. Mater.* **2012**, *22*, 4634–4667. [CrossRef]
17. Kuppan, B.; Selvam, P. Platinum-supported mesoporous carbon (Pt/CMK-3) as anodic catalyst for direct methanol fuel cell applications: The effect of preparation and deposition methods. *Prog. Nat. Sci. Mater. Int.* **2012**, *22*, 616–623. [CrossRef]
18. Bruno, M.M.; Viva, F.A.; Petruccelli, M.A.; Corti, H.R. Platinum supported on mesoporous carbon as cathode catalyst for direct methanol fuel cells. *J. Power Sources* **2015**, *278*, 458–463. [CrossRef]
19. Hung, C.-T.; Liou, Z.-H.; Veerakumar, P.; Wu, P.-H.; Liu, T.-C.; Liu, S.-B. Ordered mesoporous carbon supported bifunctional PtM (M = Ru, Fe, Mo) electrocatalysts for a fuel cell anode. *Chin. J. Catal.* **2016**, *37*, 43–53. [CrossRef]
20. Knupp, S.L.; Li, W.; Paschos, O.; Murray, T.M.; Snyder, J.; Haldar, P. The effect of experimental parameters on the synthesis of carbon nanotube/nanofiber supported platinum by polyol processing techniques. *Carbon* **2008**, *46*, 1276–1284. [CrossRef]
21. Monthioux, M. *Carbon Meta-Nanotubes: Synthesis, Properties and Applications*; Wiley: Hoboken, NJ, USA, 2011.
22. Rahsepar, M.; Pakshir, M.; Nikolaev, P.; Piao, Y.; Kim, H. A combined physicochemical and electrocatalytic study of microwave synthesized tungsten mono-carbide nanoparticles on multiwalled carbon nanotubes as a co-catalyst for a proton-exchange membrane fuel cell. *Int. J. Hydrogen Energy* **2014**, *39*, 15706–15717. [CrossRef]
23. Chiang, Y.-C.; Hsieh, M.-K.; Hsu, H.-H. The effect of carbon supports on the performance of platinum/carbon nanotubes for proton exchange membrane fuel cells. *Thin Solid Film.* **2014**, *570*, 221–229. [CrossRef]
24. Weng, B.; Xu, F.; Wu, Z.; Li, Z. Hydrogen generation from LiBH4 solution catalyzed by multiwalled carbon nanotubes supported Co–B nanocatalysts for a portable micro proton exchange membrane fuel cell application. *Int. J. Hydrogen Energy.* **2014**, *39*, 14942–14948. [CrossRef]
25. Jin, H.; Zhu, L.; Bing, N.; Wang, L.; Wang, L. No cytotoxic nitrogen-doped carbon nanotubes as efficient metal-free electrocatalyst for oxygen reduction in fuel cells. *Solid State Sci.* **2014**, *30*, 21–25. [CrossRef]

26. Kitahara, T.; Nakajima, H.; Okamura, K. Gas diffusion layers coated with a microporous layer containing hydrophilic carbon nanotubes for performance enhancement of polymer electrolyte fuel cells under both low and high humidity conditions. *J. Power Sources* **2015**, *283*, 115–124. [CrossRef]
27. Ortiz-Herrera, J.C.; Cruz-Martínez, H.; Solorza-Feria, O.; Medina, D.I. Recent progress in carbon nanotubes support materials for Pt-based cathode catalysts in PEM fuel cells. *Int. J. Hydrogen Energy* **2022**. (In Press) [CrossRef]
28. Nasrabadi, M.K.; Ebrahimi-Moghadam, A.; Kumar, R.; Nabipour, N. Electrochemical performance improvement of the catalyst of the methanol microfuel cell using carbon nanotubes. *Int. J. Chem. Eng.* **2021**, *2021*, 8894768. [CrossRef]
29. Kelly, B.T. *Physics of Graphite*; Applied Science Publishers: London, UK, 1981; p. 291.
30. Galeano, C.; Meier, J.C.; Peinecke, V.; Bongard, H.; Katsounaros, I.; Topalov, A.A.; Lu, A.; Mayrhofer, K.J.; Schüth, F. Toward highly stable electrocatalysts via nanoparticle pore confinement. *J. Am. Chem. Soc.* **2012**, *134*, 20457–20465. [CrossRef]
31. Vivekananthan, J.; Masa, J.; Chen, P.; Xie, K.; Muhler, M.; Schuhmann, W. Nitrogen-doped carbon cloth as a stable self-supported cathode catalyst for air/H2-breathing alkaline fuel cells. *Electrochim. Acta* **2015**, *182*, 312–319. [CrossRef]
32. Jha, N.; Jafri, R.I.; Rajalakshmi, N.; Ramaprabhu, S. Graphene-multi walled carbon nanotube hybrid electrocatalyst support material for direct methanol fuel cell. *Int. J. Hydrogen Energy* **2011**, *36*, 7284–7290. [CrossRef]
33. Lee, J.; Kim, K.; Park, W.I.; Kim, B.-H.; Park, J.H.; Kim, T.-H. Uniform graphene quantum dots patterned from self-assembled silica nanodots. *Nano Lett.* **2012**, *12*, 6078–6083. [CrossRef]
34. Zhang, X.; Yuan, W.; Duan, J.; Zhang, Y.; Liu, X. Graphene nanosheets modified by nitrogen-doped carbon layer to support Pt nanoparticles for direct methanol fuel cell. *Microelectron. Eng.* **2015**, *141*, 234–237. [CrossRef]
35. Li, L.; Hu, L.; Li, J.; Wei, Z. Enhanced stability of Pt nanoparticle electrocatalysts for fuel cells. *Nano Res.* **2015**, *8*, 418–440. [CrossRef]
36. Yang, H.N.; Lee, D.C.; Park, K.W.; Kim, W.J. Platinum—Boron doped grapheme intercalated by carbon black for cathode catalyst in proton exchange membrane fuel cell. *Energy* **2015**, *89*, 500–510. [CrossRef]
37. Song, C.; Gui, Y.; Xing, X.; Zhang, W. Well-dispersed chromium oxide decorated reduced graphene oxide hybrids and application in energy storage. *Mater. Chem. Phys.* **2016**, *173*, 460–466. [CrossRef]
38. Lazar, O.-A.; Marinoiu, A.; Raceanu, M.; Pantazi, A.; Mihai, G.; Varlam, M.; Enachescu, M. Reduced graphene oxide decorated with dispersed gold nanoparticles: Preparation, characterization and electrochemical evaluation for oxygen reduction reaction. *Energies* **2020**, *13*, 4307. [CrossRef]
39. Yamada, T.; Yabutani, H.; Saito, T.; Yang, C.Y. Temperature dependence of carbon nanofiber resistance. *Nanotechnology* **2010**, *21*, 265707. [CrossRef] [PubMed]
40. Oh, Y.; Kim, S.-K.; Peck, D.-H.; Jang, J.-S.; Kim, J.; Jung, D.-H. Improved performance using tungsten carbide/carbon nanofiber based anode catalysts for alkaline direct ethanol fuel cells. *Int. J. Hydrogen Energy* **2014**, *39*, 15907–15912. [CrossRef]
41. Thamer, B.M.; El-Newehy, M.H.; Barakat, N.A.M.; Abdelkareem, M.A.; Al-Deyab, S.S.; Kim, H.Y. Influence of nitrogen doping on the catalytic activity of niincorporated carbon nanofibers for alkaline direct methanol fuel cells. *Electrochim. Acta.* **2014**, *142*, 228–239. [CrossRef]
42. Giorgi, L.; Salernitano, E.; Dikonimos Makris, T.; Gagliardi, S.; Contini, V.; De Francesco, M. Innovative electrodes for direct methanol fuel cells based on carbon nanofibers and bimetallic PtAu nanocatalysts. *Int. J. Hydrogen Energy* **2014**, *39*, 21601–21612. [CrossRef]
43. Zainoodin, A.M.; Kamarudin, S.K.; Masdar, M.S.; Daud, W.R.W.; Mohamad, A.B.; Sahari, J. High power direct methanol fuel cell with a porous carbon nanofiber anode layer. *Appl. Energy* **2014**, *113*, 946–954. [CrossRef]
44. Pekala, R.W.; Farmer, J.C.; Alviso, C.T.; Tran, T.D.; Mayer, S.T.; Miller, J.M.; Dunn, B. Carbon aerogels for electrochemical applications. *J. Non-Cryst. Solids.* **1998**, *225*, 74–80. [CrossRef]
45. Job, N.; Marie, J.; Lambert, S.; Berthon-Fabry, S.; Achard, P. Carbon xerogels as catalyst supports for PEM fuel cell cathode. *Energy Convers. Manag.* **2008**, *49*, 2461–2470. [CrossRef]
46. Sharma, C.; Kulkarni, M.; Sharma, A.; Madou, M. Synthesis of carbon xerogel particles and fractal-like structures. *Chem. Eng. Sci.* **2009**, *64*, 1536–1543. [CrossRef]
47. Liu, B.; Creager, S. Carbon xerogels as Pt catalyst supports for polymer electrolyte membrane fuel-cell applications. *J. Power Sources* **2010**, *195*, 1812–1820. [CrossRef]
48. Calderón, J.C.; Mahata, N.; Pereira, M.F.R.; Figueiredo, J.L.; Fernandes, V.R.; Rangel, C.M.; Calvillo, L.; Lázaro, M.J.; Pastor, E. Pt–Ru catalysts supported on carbon xerogels for PEM fuel cells. *Int. J. Hydrogen Energy* **2012**, *37*, 7200–7211. [CrossRef]
49. Gao, X.; Omosebi, A.; Landon, J.; Liu, K. Surface charge enhanced carbon electrodes for stable and efficient capacitive deionization using inverted adsorption—Desorption behavior. *Energy Environ. Sci.* **2015**, *8*, 897–909. [CrossRef]
50. Hayashida, T.; Pan, L.; Nakayama, Y. Mechanical and electrical properties of carbon tubule nanocoils. *Physica B* **2002**, *323*, 352–353. [CrossRef]
51. Sevilla, M.; Sanchís, C.; Valdés-Solís, T.; Morallón, E.; Fuertes, A.B. Highly dispersed platinum nanoparticles on carbon nanocoils and their electrocatalytic performance for fuel cell reactions. *Electrochim. Acta* **2009**, *54*, 2234–2238. [CrossRef]
52. Jafri, R.I.; Rajalakshmi, N.; Ramaprabhu, S. Nitrogen-doped multi-walled carbon nanocoils as catalyst support for oxygen reduction reaction in proton exchange membrane fuel cell. *J. Power Sources* **2010**, *195*, 8080–8083. [CrossRef]
53. Shaikjee, A.; Coville, N.J. The synthesis, properties and used of carbon materials with helical morphology. *J. Adv. Res.* **2012**, *3*, 195–223. [CrossRef]

54. Suda, Y.; Ozaki, M.; Tanoue, H.; Takikawa, H.; Ue, H.; Shimizu, K. Supporting PtRu catalysts on various types of carbon nanomaterials for fuel cell applications. *J. Phys. Conf. Ser.* **2013**, *433*, 012008. [CrossRef]
55. Tang, S.; Huangfu, H.; Dai, Z.; Sui, L.; Zhu, Z. Preparation of Fe-N-carbon nanocoils as catalyst for oxygen reduction reaction. *Int. J. Electrochem. Sci.* **2015**, *10*, 7180–7191.
56. Mohammad, K.; Forouzan, A.; Hamid Reza Lotfi Zadeh, Z.; Omid, S.; Ezzatollah, N. Electrocatalytic performance of Pt/Ru/Sn/W fullerene electrode for methanol oxidation in direct methanol fuel cell. *J. Fuel Chem. Technol.* **2013**, *41*, 91–95. [CrossRef]
57. Zhang, Q.; Bai, Z.; Shi, M.; Yang, L.; Qiao, J.; Jiang, K. High-efficiency palladium nanoparticles supported on hydroxypropyl-b-cyclodextrin modified fullerene [60] for ethanol oxidation. *Electrochim. Acta* **2015**, *177*, 113–117. [CrossRef]
58. Rambabu, G.; Bhat, S.D. Sulfonated fullerene in SPEEK matrix and its impact on the membrane electrolyte properties in direct methanol fuel cells. *Electrochim. Acta* **2015**, *176*, 657–669.
59. Borgohain, R.; Yang, J.; Selegue, J.P.; Kim, D.Y. Controlled synthesis, efficient purification, and electrochemical characterization of arc-discharge carbon nano-onions. *Carbon* **2014**, *66*, 272–284. [CrossRef]
60. Dhand, V.; Prasad, J.S.; Rao, M.V.; Bharadwaj, S.; Anjaneyulu, Y.; Jain, P.K. Flame synthesis of carbon nano onions using liquefied petroleum gas without catalyst. *Mater. Sci. Eng. C* **2013**, *33*, 758–762. [CrossRef]
61. Zhu, S.; Xu, G. Single-walled carbon nanohorns and their applications. *Nanoscale* **2010**, *2*, 2538–2549. [CrossRef]
62. Unni, S.M.; Bhange, S.N.; Illathvalappil, R.; Mutneja, N.; Patil, K.R.; Kurungot, S. Nitrogen-induced surface area and conductivity modulation of carbon nanohorn and its function as an efficient metal-free oxygen reduction electrocatalyst for anion-exchange membrane fuel cells. *Small* **2015**, *11*, 352–360. [CrossRef]
63. Ghosh, S.; Das, S.; Mosquera, M.E.G. Conducting polymer-based nanohybrids for fuel cell application. *Polymers* **2020**, *12*, 2993. [CrossRef]
64. Takahashi, K.; Koda, R.; Kakinuma, K.; Uchida, M. Improvement of cell performance in low-pt-loading PEFC cathode catalyst layers with Pt/Ta-$SnO_2$ prepared by the electrospray method. *J. Electrochem. Soc.* **2017**, *164*, F235. [CrossRef]
65. Tan, Y.; Matsui, H.; Ishiguro, N.; Uruga, T.; Nguyen, D.-N.; Sekizawa, O.; Sakata, T.; Maejima, N.; Higashi, K.; Dam, H.C.; et al. Pt−Co/C cathode catalyst degradation in a polymer electrolyte fuel cell investigated by an infographic approach combining threedimensional spectroimaging and unsupervised learning. *J. Phys. Chem. C* **2019**, *123*, 18844–18853. [CrossRef]
66. Osmieri, L.; Cullen, D.A.; Chung, H.T.; Ahluwalia, R.K.; Neyerlin, K.C. Durability evaluation of a Fe–N–C catalyst in polymer electrolyte fuel cell environment via accelerated stress tests. *Nano Energy* **2020**, *78*, 105209. [CrossRef]
67. Inoue, G.; Takenaka, S. Design of interfaces and phase interfaces on cathode catalysts for polymer electrolyte fuel cells. *Chem. Lett.* **2021**, *50*, 136–143. [CrossRef]
68. Hiramatsu, M.; Hori, M. *Carbon Nanowalls*; Springer: Wien, Austria, 2010. [CrossRef]
69. Hiramatsu, M.; Kondo, H.; Hori, M. Graphene Nanowalls. In *New Progress on Graphene Research*; Gong, J.R., Ed.; Intech Open Ltd.: London, UK, 2013; Chapter 9; pp. 235–260. [CrossRef]
70. Ichikawa, T.; Shimizu, N.; Ishikawa, K.; Hiramatsu, M.; Hori, M. Synthesis of isolated carbon nanowalls via high-voltage nanosecond pulses in conjunction with $CH_4/H_2$ plasma enhanced chemical vapor deposition. *Carbon* **2020**, *161*, 403. [CrossRef]
71. Yerlanuly, Y.; Christy, D.; Nong, N.-V.; Kondo, H.; Alpysbayeva, B.; Nemkayeva, R.; Kadyr, M.; Ramazanov, T.; Gabdullin, M.; Batryshev, D.; et al. Synthesis of carbon nanowalls on the surface of nanoporous alumina membranes by RI-PECVD method. *Appl. Surf. Sci.* **2020**, *523*, 146533. [CrossRef]
72. Shin, S.-C.; Yoshimura, A.; Matsuo, T.; Mori, M.; Tanimura, M.; Ishihara, A.; Ota, K.; Tachibana, M. Carbon nanowalls as platinum support for fuel cells. *J. Appl. Phys.* **2011**, *110*, 104308. [CrossRef]
73. Ashikawa, A.; Yoshie, R.; Kato, K.; Miyazawa, K.; Murata, H.; Hotozuka, K.; Tachibana, M. Pt nanoparticles supported on carbon nanowalls with different domain sizes, for oxygen reduction reaction. *J. Appl. Phys.* **2015**, *118*, 214303. [CrossRef]
74. Hiramatsu, M.; Mitsuguchi, S.; Takeyoshi, H.; Kondo, H.; Hori, M.; Kano, H. Fabrication of carbon nanowalls on carbon fiber paper for fuel cell application. *Jpn. J. Appl. Phys.* **2013**, *52*, 01AK03. [CrossRef]
75. Imai, S.; Kondo, H.; Hyungjun, C.; Kano, H.; Ishikawa, K.; Sekine, M.; Hiramatsu, M.; Ito, M.; Hori, M. High-durability catalytic electrode composed of Pt nanoparticles-supported carbon nanowalls synthesized by radical-injection plasma-enhanced chemical vapor deposition. *J. Phys. D* **2017**, *50*, 40LT01. [CrossRef]
76. Imai, S.; Kondo, H.; Hyungjun, C.; Ishikawa, K.; Tsutsumi, T.; Sekine, M.; Hiramatsu, M.; Hori, M. Pt nanoparticle-supported carbon nanowalls electrode with improved durability for fuel cell applications using $C_2F_6/H_2$ plasma-enhanced chemical vapor deposition. *Appl. Phys. Express* **2018**, *12*, 015001. [CrossRef]
77. Imai, S.; Kondo, H.; Hyungjun, C.; Ishikawa, K.; Tsutsumi, T.; Sekine, M.; Hiramatsu, M.; Hori, M. Effects of three-dimensional structure on electrochemical oxygen reduction characteristics of Pt-nanoparticle-supported carbon nanowalls. *J. Phys. D* **2019**, *52*, 105503. [CrossRef]
78. Lehmann, K.; Yurchenko, O.; Urban, G. Carbon nanowalls for oxygen reduction reaction in bio fuel cells. *J. Phys. Conf. Ser.* **2014**, *557*, 012008. [CrossRef]
79. Slobodian, P.; Riha, P.; Kondo, H.; Cvelbar, U.; Olejnik, R.; Matyas, J.; Sekine, M.; Hori, M. Transparent elongation and compressive strain sensors based on aligned carbon nanowalls embedded in polyurethane. *Sens. Actuator A Phys.* **2020**, *306*, 111946. [CrossRef]
80. Tomatsu, M.; Hiramatsu, M.; Foord, J.S.; Kondo, H.; Ishikawa, K.; Sekine, M.; Takeda, K.; Hori, M. Hydrogen peroxide sensor based on carbon nanowalls grown by plasma-enhanced chemical vapor deposition. *Jpn. J. Appl. Phys.* **2017**, *56*, 06HF03. [CrossRef]

81. Tomatsu, M.; Hiramatsu, M.; Kondo, H.; Ishikawa, K.; Tsutsumi, T.; Sekine, M.; Hori, M. Electrochemical Reaction in Hydrogen Peroxide and Structural Change of Platinum Nanoparticle-Supported Carbon Nanowalls Grown Using Plasma-Enhanced Chemical Vapor Deposition. *C* **2019**, *5*, 7. [CrossRef]
82. Slobodian, P.; Cvelbar, U.; Riha, P.; Olejnik, R.; Matyas, J.; Filipič, G.; Watanabe, H.; Tajima, S.; Kondo, H.; Sekine, M.; et al. High sensitivity of a carbon nanowall-based sensor for detection of organic vapours. *RSC Adv.* **2015**, *5*, 90515. [CrossRef]
83. Ichikawa, T.; Tanaka, S.; Kondo, H.; Ishikawa, K.; Tsutsumi, T.; Sekine, M.; Hori, M. Effect of electrical stimulation on proliferation and bone-formation by osteoblast-like cells cultured on carbon nanowalls scaffolds. *Appl. Phys. Express* **2019**, *12*, 025006. [CrossRef]
84. Ohta, T.; Ito, H.; Ishikawa, K.; Kondo, H.; Hiramatsu, M.; Hori, M. Atmospheric pressure plasma-treated carbon nanowalls surface-assisted laser desorption/ionization time-of-flight mass spectrometry (CNW-SALDI-MS). *C* **2019**, *5*, 40. [CrossRef]
85. Sakai, R.; Ichikawa, T.; Kondo, H.; Ishikawa, K.; Shimizu, N.; Ohta, T.; Hiramatsu, M.; Hori, M. Effects of carbon nanowalls (CNWs) substrates on soft ionization of low-molecular-weight organic compounds in surface-assisted laser desorption/ionization mass spectrometry (SALDI-MS). *Nanomaterials* **2021**, *11*, 262. [CrossRef]
86. Vielstich, W.; Gasteiger, H.A.; Lamm, A. *Handbook of Fuel Cells—Fundamentals, Technology and Applications*; John Wiley & Sons, Ltd.: Hoboken, NJ, USA, 2003.
87. Schneider, C.A.; Rasband, W.S.; Eliceiri, K.W. NIH image to imageJ: 25 years of image analysis. *Nat. Methods* **2012**, *9*, 671–675. [CrossRef] [PubMed]